

Reinforcement Learning Based Optimal Battery Control Under Cycle-based Degradation Cost

Kyung-bin Kwon, *Student Member, IEEE*, and Hao Zhu, *Senior Member, IEEE*

Abstract—Battery energy storage systems are providing increasing level of benefits to power grid operations by decreasing the resource uncertainty and supporting frequency regulation. Thus, it is crucial to obtain the optimal policy for battery to efficiently provide these grid-services while accounting for its degradation cost. To solve the optimal battery control (OBC) problem using the powerful reinforcement learning (RL) algorithms, this paper aims to develop a new representation of the cycle-based battery degradation model according to the rainflow algorithm. As the latter depends on the full trajectory, existing work has to rely on linearized approximation for converting it into instantaneous terms for the Markov Decision Process (MDP) based formulation. We propose a new MDP form by introducing additional state variables that can easily keep track of past switching points for determining the cycle depth. The proposed degradation model allows to adopt the powerful deep Q-Network (DQN) based RL algorithm to efficiently search for the OBC policy. Numerical tests using real market data have demonstrated the performance improvements of the proposed cycle-based degradation model in enhancing the battery operations while mitigating its degradation, as compared to earlier work using the linearized approximation.

Index Terms—Energy storage, reinforcement learning, battery degradation, rainflow algorithm, deep Q-networks (DQN)

I. INTRODUCTION

Battery energy storage systems as flexible resources are a key technology to enable the electricity infrastructure to achieve the low-carbon or carbon-neutral vision in future [1], [2]. Battery systems can be used to reduce the energy costs of the owners' via energy arbitrage [3], while contributing to the grid's power balance through participation in ancillary services [4]. It is crucial to develop effective strategies for real-time battery operations in order to utilize its flexibility potentials to mitigate the increasing uncertainty introduced by renewable or non-controllable generation.

The optimal battery control (OBC) problem for determining the (dis)charging policies has been popularly considered to reduce a combination of certain operational costs, such as the net cost for electricity usage, frequency regulation (FR) penalty, and peak-shaving cost; see e.g., [5]–[7]. Additional problem consideration includes the precise circuit model of battery [8] or the network constraints on grid voltage [9]. Due to the dynamics of inputs such as prices or load demands, the OBC problem is challenged by the unknown uncertainty of future signals, and model-predictive control [10] or stochastic

optimization [11] has been widely used to address it. More importantly, battery's cycle life as modeled by the degradation cost is especially needed with the participation in FR or other fast services; see e.g., [5], [7]. Unlike other costs that mostly depend on the instantaneous battery status, the modeling of battery degradation is *cycle-based* according to the full trajectory of battery's state of charge (SoC). Specifically, it requires the identification of all charging/discharging cycles using the so-termed *rainflow* algorithm [12]. Hence, it is typically more complicated to include the degradation cost into the design of OBC algorithms as shown by [5], [7].

Recent advances on reinforcement learning (RL) [13] enable the effective search of optimal policies directly using real data samples to address the uncertainty issue in dynamical systems. This data-driven framework helps to bypass the hurdles in formulating the complex models of system dynamics or estimating the statistical information on the uncertainty. Specifically for the OBC problem, it allows to flexibly incorporate a variety of operational objectives, and several RL techniques have been widely used, such as the Deep Q-Network (DQN) [14], SARSA [15] and $TD(\lambda)$ -learning [16]. However, a majority of these techniques have not considered the battery degradation cost, as its cycle-based model is difficult to include by the RL formulation. Very recently, [17] has developed a linearized approximation for the cycle-based degradation cost, which converts it to an instantaneous degradation coefficient that can be used by the RL algorithms. Nevertheless, the accuracy of this approximation method depends on a given sample trajectory based on which the linearization is performed. The resultant modeling mismatch can limit the RL iterations from finding the best policy within the full search space. Thus, it is still an open problem on effectively incorporating the accurate battery degradation cost into the search of optimal OBC policy.

The goal of our work is to develop a modeling approach to precisely represent the battery degradation cost and use it for the design of RL-based OBC algorithm. The main modeling challenge lies in that the degradation cost is determined by the battery's full (dis)charging trajectory throughout the operational horizon. Based on the rainflow algorithm, the complex process of material fatigue is associated with the stress level of each individual charging or discharging cycle [18]. Thus, the degradation cost is an exponentially increasing function of cycle depth [12], and the latter strongly depends on the past trajectory of battery status. This leads to a pronounced mismatch between this degradation model and the Markov Decision Process (MDP) form used by RL algorithms, as the latter would represent the problem objective as functions of instantaneous states only. The aforementioned approach

This work has been supported by NSF Grants 1802319 and 1952193.

The authors are with the Department of Electrical & Computer Engineering, The University of Texas at Austin, 2501 Speedway, Austin, TX, 78712, USA; Emails: {kwon8908kr, haozhu}@utexas.edu.

of linearizing the degradation cost as in [17], [19] fails to recognize this exponential relation with the cycle depth, and unfortunately can lead to deep (dis)charging cycles that may not be profitable. To this end, we have shown that it is possible to keep track of the battery cycles by augmenting the state with the more recent switching points (SPs) along the trajectory. These critical transition points between charging and discharging sessions are extremely useful for identifying the correct cycle depth based on the rainflow algorithm. In addition, they allow for decomposing the degradation cost of a full (dis)charging cycle into incremental differences between consecutive time instances in the form of instantaneous cost. This novel representation of battery degradation cost helps to deploy state-of-the-art RL algorithms to learn the OBC policy. We have used the DQN technique to search for the parameters of the action-value function, or Q-function, associated with the resultant MDP form.

To sum up, the main contribution of the present paper is two-fold. First, we have developed an instantaneous cost modeling of the battery degradation with guaranteed equivalence to the original cycle-based representation. Second, the proposed degradation cost is successfully applied to form an MDP problem, allowing to develop efficient RL algorithms for effective search of OBC policies. Our numerical tests using real data of electricity prices and FR signals have validated the performance improvement of the proposed cycle-based cost model in accurately representing battery degradation and effectively generating profit-seeking OBC policies.

The rest of the paper is organized as follows. Section II introduces the key variables for modeling the battery control problem into the MDP form. In Section III, we model the cycle-based degradation cost using the rainflow algorithm, and develop a new approach to represent it as instantaneous MDP cost through state augmentation. Section IV formalizes the OBC problem and presents the DQN method as the RL solution technique. Numerical results using real-world datasets are presented in Section V to validate the effectiveness and performance improvement of the proposed degradation model, as compared to earlier approach using linearized approximation. Finally, the paper is wrapped up in Section VI.

II. SYSTEM MODELING

Optimal battery control (OBC) aims to maximize the economic pay-off while accounting for the battery degradation cost. The pay-off is from energy market participation and also the provision of FR service, as discussed later. One notable feature of the present work is the consideration of battery degradation cost, which can greatly increase the life-cycle under any general pay-off model [5]. A list of symbol notation and description is tabulated in Table I.

To determine the battery's effective (dis)charging power $b_t \in [\underline{b}, \bar{b}]$ at each discrete-time instance $t = 0, 1, \dots$, we introduce a list of state variables based on battery status or external inputs.

- $c_t \in [\underline{c}, \bar{c}]$: normalized state of charge (SoC) of the battery;
- p_t : electricity market price;

TABLE I
LIST OF SYMBOLS

Notation	Description
c_t	state of charge (SoC) of the battery
\bar{c}, \underline{c}	maximum/minimum capacity of the battery
p_t	electricity market price
f_t	frequency regulation (FR) signal
s_t	battery full state
a_t	battery charging/discharging action
b_t	battery charging/discharging power
γ	discount factor
\mathcal{T}	the exploration time-horizon
h_t^e	net cost for electricity usage
h_t^f	frequency regulation penalty
h_t^d	battery degradation cost
δ	frequency regulation penalty coefficient
$\Phi(d)$	degradation cost for a cycle of depth d
α_d, β	degradation coefficient based on battery types
$c_t^{(0)}, c_t^{(1)}, c_t^{(2)}$	SoC level of switching points (SPs)

- f_t : frequency regulation (FR) signal.

Note that the SoC is normalized by the maximum capacity; i.e., $c_t \in [0, 1]$. It is also an internal battery state affected by the past actions $\{b_\tau\}$, whereas the other states are received from grid operators and thus are not directly action-dependent.

To leverage reinforcement learning algorithms for this problem, we consider it as a Markov Decision Process (MDP) [20, Ch. 3] denoted by a tuple $(\mathcal{S}, \mathcal{A}, \mathcal{P}, \mathcal{R}, \gamma)$, as detailed here.

State space \mathcal{S} contains the set of feasible values for the system state s_t , including both the SoC c_t , and the other inputs p_t and f_t which affect the economic benefits. Additional state variables may be included if other operational objectives, such as peak shaving, would be considered. State dynamics need to follow the Markov property as discussed soon.

Action space \mathcal{A} includes the set of decisions that battery can take. One simple example is to use

$$a_t \in \mathcal{A} = \{-1(\text{discharge}), 0(\text{do nothing}), 1(\text{charge})\}. \quad (1)$$

Based on the action a_t , the normalized (dis)charging power $b_t \in [-1, 1]$ is set to be

$$b_t = \begin{cases} \bar{b} & \text{if } a_t = 1, \bar{c} - c_t \geq \bar{b} \\ \underline{b} & \text{if } a_t = -1, \underline{c} - c_t \leq \underline{b} \\ 0 & \text{otherwise} \end{cases} \quad (2)$$

which considers the maximum (dis)charging only for simplicity. It can be easily generalized to a multi-level charging rate with $|\mathcal{A}| > 3$. Continuous actions that directly determine $b_t = a_t$ are also possible. This paper focuses on the simple discrete case in (1), but the proposed algorithm can be easily extended to more general cases as well.

Transition kernel $\mathcal{P} : \mathcal{S} \times \mathcal{A} \times \mathcal{S} \rightarrow [0, 1]$ captures the system dynamics under the Markov property [20, Ch. 3]. For the input states such as price p_t , we assume $\Pr(p_{t+1} | \{p_\tau\}_{\tau=1}^t) = \Pr(p_{t+1} | p_t)$; and similarly for f_t . This is reasonable as the market price has very short-term memory [21], while FR signal f_t can be modeled as a random walk [22]. A longer memory is possible too; such as the prices that follow $\Pr(p_{t+1} | \{p_\tau\}_{\tau=1}^t) = \Pr(p_{t+1} | p_t, p_{t-1})$. In this case, both p_t

and p_{t-1} are included as the part of the state per time t to satisfy the Markov transition property.

Using the normalized b_t in (2), the SoC state c_t changes according to action a_t , given by

$$c_{t+1} = c_t + b_t, \text{ with } b_t \text{ given in (2)}. \quad (3)$$

For general action space with any $b_t \in [\underline{b}, \bar{b}]$, c_t is updated as

$$c_{t+1} = \begin{cases} \bar{c} & \text{if } \bar{c} - c_t \leq b_t \\ \underline{c} & \text{if } \underline{c} - c_t \geq b_t \\ c_t + b_t & \text{otherwise} \end{cases}. \quad (4)$$

Reward function $\mathcal{R} : \mathcal{S} \times \mathcal{A} \rightarrow \mathbb{R}$ captures the learning objective. Notably, it is always the accumulated reward consisting of *instantaneous* terms, where per time t the latter only depends on the current state and action as

$$r_t = r_t(s_t, a_t) \quad (5)$$

In the following we will formulate the objective function as *costs* h_t as negative reward, where the instantaneous property of reward function will be ensured by introducing additional state variables.

Discount factor $\gamma \in (0, 1]$ is a constant to accumulate the total reward along the time horizon. Smaller γ values imply that future rewards are less important than current ones at a discounted rate [20, Ch. 3]. As we adopt a finite exploration time-horizon $\mathcal{T} = [1, \dots, T]$ for the OBC problem, for simplicity $\gamma = 1$ will be used.

III. MODELING OF BATTERY DEGRADATION COST

We consider three types of operational cost related to battery operations. The energy cost relates to the electricity price according to (dis)charging, while the FR cost is based on its fast-varying flexibility. Under a contract of providing FR service, the battery would follow the f_t signal sent by the market operator as much as possible [5]. These two costs can be simply obtained by the state variables discussed so far. First, the net cost for electricity usage under (dis)charging power b_t can be represented as

$$h_t^e(p_t, b_t) = p_t b_t, \quad \forall t \in \mathcal{T}. \quad (6)$$

Second, using a penalty coefficient δ for deviation from FR signal f_t , one can form

$$h_t^f(f_t, b_t) = \delta |f_t - b_t|, \quad \forall t \in \mathcal{T}. \quad (7)$$

Remark 1. (Fast frequency regulation signal) *In practice, the FR signal may be much faster than the sampling period of the OBC problem. For example, the real-time price is typically updated every 5 minutes, which can be chosen as the sampling period, while the FR signal may be at 1-minute rate. To deal with this difference, we can down-sample the actual FR signal to attain $\{f_t\}$ at the problem sampling rates for the search of optimal policy during the training phase. For testing and implementing the resultant optimal policy, the original fast FR signal can be instead used to better evaluate the performance of the proposed RL algorithm.*

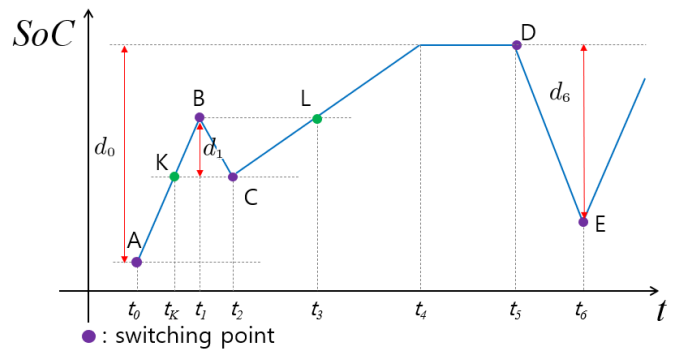


Fig. 1. An example of battery SoC trajectory used for modeling the battery degradation cost based on the rainflow algorithm.

Compared to these two cost functions expressed using instantaneous state/action variables, the *cycle-based* degradation cost is more complicated to model, and thus the key challenge becomes to effectively decompose it into instantaneous terms for each t . The aging of battery cells mainly depends on material fatigue as a result of (dis)charging cycles of the SoC trajectory, especially due to following the FR signal [5]. The rainflow algorithm [12] is widely used as an extremely effective approach for this modeling. Fig. 1 illustrates an example of battery SoC trajectory which consists of several charging and discharging cycles. The switching points (SPs), labeled by $A - E$, correspond to the transitions between charging and discharging and will be used for identifying the cycles by rainflow algorithm.

For example, the trajectory $A - B - C - D$ consists of a long charging cycle with a small discharging part from $B - C$. The respective depths of these two cycles, defined as the absolute SoC differences between the start and end SPs, are d_0 and d_1 . As d_1 is smaller than the difference between $A - B$ and that between $C - D$, this trajectory is thus divided into the *full cycle* from $K - B - C$ of depth d_1 and the other *half cycle* from $A - K(C) - D$ of depth d_0 . This is the so-called rainflow condition which uses *four consecutive SPs* to determine the exact cycles and their depths. The degradation cost associated with each cycle of depth $d \geq 0$ is computed as

$$\Phi(d) = \alpha_d e^{\beta d} \quad (8)$$

with positive constant coefficients α_d and β based on battery types. Recalling the normalized SoC $c_t \in [0, 1]$, we have the cycle depth $d \in [0, 1]$ as well. Note that for any pair in $\mathcal{D} := \{(d_1, d_2) : d_1, d_2 \geq 0, d_1 + d_2 \leq 1\}$, we can show that $e^{(d_1+d_2)} \leq e^{d_1} + e^{d_2}$. This is because the maximum value of the function $g(d_1, d_2) := e^{(d_1+d_2)} - e^{d_1} - e^{d_2}$ for the simplex \mathcal{D} equals to $(e - 2e^{0.5}) < 0$, which is attained at $(d_1, d_2) = (0.5, 0.5)$. Thus, to reduce the degradation cost a single (dis)charging cycle that is longer and deeper is typically preferred, as opposed to the combination of multiple shorter cycles. This intuitive rule under cycle-based degradation model will be demonstrated later on in numerical tests.

Unfortunately, this cycle-based degradation cost is determined by the full SoC trajectory and does not follow the accumulated form of instantaneous terms as in (5). To address this issue, recent work [17] has developed a *linearized*

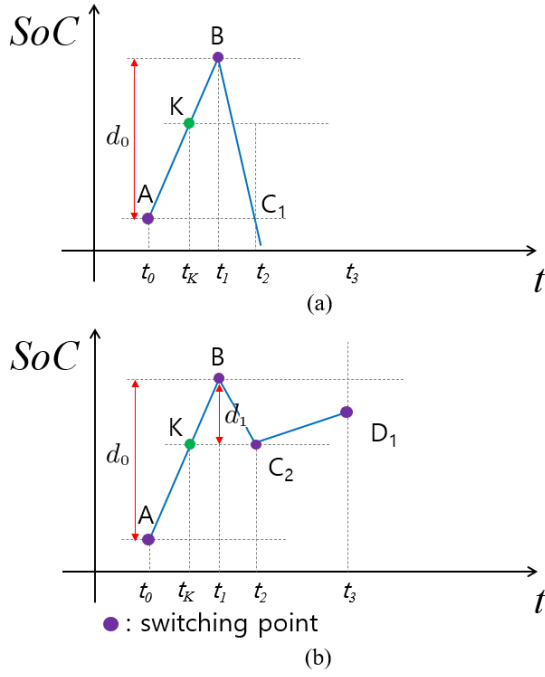


Fig. 2. Two cases of rainflow condition not satisfied: (a) case NR_a and (b) case NR_b .

approximation model for it. Specifically, using a given sample SoC trajectory over \mathcal{T} , one can first determine a degradation coefficient α_d as

$$\alpha_d = \frac{\sum_{i=0}^{\bar{N}} \Phi(\bar{d}_i)}{\sum_{t=0}^T |\bar{b}_t|} \quad (9)$$

by averaging the total degradation costs of the $(\bar{N} + 1)$ cycles over the accumulative absolute charging power throughout a given sample trajectory. This way, the instantaneous degradation cost for any new SoC trajectory is approximated by

$$h_t^d(b_t) \cong -\alpha_d |b_t|. \quad (10)$$

This linearized degradation cost model can be easily computed once α^d is known. However, this approximation inexplicitly assumes that the new trajectory should be very similar to the given sample trajectory for computing α_d . To implement the RL algorithm later on, the coefficient α_d will be updated using the most recent trajectory during the sampling process. Nonetheless, as an approximation it does not represent the actual cycle-based degradation cost and thus limits the RL algorithm's search for the best SoC trajectory.

We develop a new approach to accurately model the cycle-based degradation cost by augmenting the state s_t with the last three SPs before time t . Intuitively, the last three SPs are needed to check for the rainflow condition when a new SP arises, as illustrated by Fig. 1. Three additional state variables, $c_t^{(0)}$, $c_t^{(1)}$, and $c_t^{(2)}$, are included to keep record of the last three SPs per time t , from the oldest to the latest. Note that they may overlap if there are less than three SPs before time t . For example, at point K in Fig. 1, these three SP states all equal to the SoC of point A ; and similarly for point C , we have $c_t^{(1)} = c_t^{(2)}$ equal to the SoC of B . The latest SP's SoC $c_t^{(2)}$

TABLE II
TRANSITIONS OF STATE VARIABLES AT TIME t IDENTIFIED AS A NEW SP

Next state	NR_a	NR_b	RA
$c_{t+1}^{(0)}$	$c_t^{(1)}$	$c_t^{(1)}$	$c_t^{(0)}$
$c_{t+1}^{(1)}$	$c_t^{(1)}$	$c_t^{(2)}$	$c_t^{(0)}$
$c_{t+1}^{(2)}$	$c_t^{(1)}$	c_t	$c_t^{(0)}$

can be used to identify if the current instance t is a new SP, using the rule

$$b_t(c_t - c_t^{(2)}) < 0. \quad (11)$$

If (11) holds, we have a new SP and will update $\{c_t^{(i)}\}$ based on whether the rainflow condition is satisfied.

To update $\{c_t^{(i)}\}$, Fig. 2 illustrates two cases where the rainflow condition is not satisfied. Fig. 2(a) shows the SoC of the point C_1 is not within the range between A and B , while Fig. 2(b) indicates the SoC of the new SP D is within the range between C_2 and B . These cases are denoted by cases NR_a and NR_b , respectively. In either case, the SoC of the latest SP will be included by updating $c_{t+1}^{(2)} \leftarrow c_t^{(2)}$ and $c_{t+1}^{(1)} \leftarrow c_t^{(1)}$ and setting $c_{t+1}^{(2)} = c_t$. As discussed earlier, Fig. 1 shows an example of rainflow condition being satisfied at SP D , which will be denoted by the case RA . This is because at SP D : i) the third SP C lies between the first two SPs A and B ; and ii) the current SoC at SP D exceeds the range between the latest two SPs B and C . Hence, the trajectory $A - B - C - D$ is divided in to the long half-cycle $A - K - C - L$, and another full-cycle $K - B - C$ of depth d_1 . After the RA case is satisfied, the two SPs B and C will be removed from the record. The SoC state updates for all three cases are summarized in Table II.

Interestingly, the state transitions in Table II also allow for decomposing the cycle-based degradation cost into instantaneous difference term for each instance t . As the cycle depth changes according to b_t only, the degradation cost in (8) can be modeled by accumulating the following incremental term per time t :

$$h_t^d(b_t, c_t, c_t^{(2)}) = \alpha_d e^{\beta |c_t + b_t - c_t^{(2)}|} - \alpha_d e^{\beta |c_t - c_t^{(2)}|}. \quad (12)$$

Basically, the instantaneous degradation model in (12) accounts for difference of $\Phi(\cdot)$ due to the change of cycle-depth, which can be computed based on the latest SP state $c_t^{(2)}$.

Although (12) holds for any $t \in \mathcal{T}$, there is some notable exception for the case RA . As shown in Fig. 1, before reaching the point L , the trajectory $K - B$ would be considered as part of the cycle $A - B$, while the cycle $C - L$ is unrelated to other cycles. However, upon reaching point L , the cycle depths of both $A - B$ and the continuing cycle $C - L$ exceed that of $B - C$, and thus rainflow condition is satisfied. As a result, $K - B$ constitutes as a short charging cycle which is no longer part of $A - B$, whereas $C - L$ becomes part of the long half cycle $A - K - C - L$. Regardless of this exceptional scenario for case RA , the model in (12) holds for computing the instantaneous change of cycle-based degradation cost from any time t to $t + 1$, which will facilitate the development of RL-based OBC algorithm next.

IV. OPTIMAL BATTERY CONTROL ALGORITHM

Thanks to our proposed model of instantaneous degradation cost, we can include to the MDP form for representing the rainfall based degradation cost. First, each state is given by

$$s_t = [p_t, f_t, c_t, c_t^{(0)}, c_t^{(1)}, c_t^{(2)}], \quad \forall t \in \mathcal{T} \quad (13)$$

which is used to determine the action a_t based on the policy of interest. The transition kernel \mathcal{P} now includes the updates in Table II, while the instantaneous reward is given by

$$r_t(s_t, a_t) = -h_t^e - h_t^f - h_t^d, \quad \forall t \in \mathcal{T}. \quad (14)$$

The battery control problem now becomes to determine the best policy π for forming the action as $a_t \sim \pi(s_t)$ with s_t given in (13). To simplify the policy search, we are particularly interested in the set of parameterized policies given by $\pi_\theta(\cdot) = \pi(\cdot; \theta)$, with parameter θ optimized through

$$\max_{\theta} \mathbb{E}_{\pi_\theta} \left[\sum_{t=1}^T \gamma^t r_t(s_t, a_t) \right]. \quad (15)$$

To solve (15), we can adopt certain RL algorithms to search for the optimal parameter θ ; see e.g., [13]. We use the deep Q-networks (DQNs) [20, Ch. 9] here as a popular RL approach based on nonlinear neural network modeling. Accordingly, the parameter θ represents the DQN weights to be learned, and the DQN is used to obtain the so-termed Q-network that models the MDP's *action-value*, or *Q-function*, namely the expected total future reward under a given pair of state and action:

$$Q(s_t, a_t) := \mathbb{E}_{\pi_\theta} \left[\sum_{\tau=t}^T \gamma^{(\tau-t)} r_\tau(s_\tau, a_\tau) \mid s_t, a_t \right]. \quad (16)$$

For the optimal Q-function, the Bellman optimality condition [13] states that:

$$Q^*(s_t, a_t) = r_t(s_t, a_t) + \gamma \mathbb{E}_{s_{t+1}} \left[\max_{a_{t+1}} Q^*(s_{t+1}, a_{t+1}) \mid s_t, a_t \right]. \quad (17)$$

To find the optimal Q^* , we parameterize the Q-network using θ as the NN weights, as denoted by $Q(s_t, a_t; \theta)$. The Bellman optimality in (17) can be used to develop iterative *gradient descent* updates to obtain the best θ . At each update, the Q-network on the right-hand side of (17) is kept constant as the *target network*, whereas the other one is varied to minimize the difference between both sides. Letting θ' denote the latest NN weights, we design the loss function for DQN training as the expected squared difference:

$$\mathcal{L}(\theta) = \mathbb{E}_{\{s_t, a_t, s_{t+1}\}} \left[\left(r_t + \gamma \max_{a_{t+1}} Q(s_{t+1}, a_{t+1}; \theta') - Q(s_t, a_t; \theta) \right)^2 \right]. \quad (18)$$

To minimize $\mathcal{L}(\theta)$, one can need to compute its gradient over the parameter θ given by

$$\nabla_{\theta} \mathcal{L}(\theta) = \mathbb{E}_{\{s_t, a_t, s_{t+1}\}} \left[-2 \left(r_t + \gamma \max_{a_{t+1}} Q(s_{t+1}, a_{t+1}; \theta') - Q(s_t, a_t; \theta) \right) \nabla_{\theta} Q(s_t, a_t; \theta) \right]. \quad (19)$$

Each gradient-based update relies on the estimate from sampling the trajectory such that the expectation in (19) is replaced by the sample average. To this end, the action a_t is sampled for given state s_t based on θ' as $a_t^* = \arg \max_{a_t} Q(s_t, a_t; \theta')$, $\forall t$. To ensure adequate exploration of the state space, the ϵ -greedy method [20, Ch. 2] can be used to randomize the action by selecting a_t^* with probability $(1 - \epsilon)$ at every time. The value of ϵ would decrease as the DQN updates continue, typically at an exponential decreasing rate $\kappa \in (0, 1)$. This method can improve the exploration process at the beginning phase while eventually picking the optimal actions to attain convergence.

To accelerate the DQN implementation, we introduce two additional techniques. First, we use the *experience replay* method [23] to accelerate the computation time by storing all the past samples in the memory $\mathfrak{D} := \{(s_t, a_t, s_{t+1}, r_t)\}$ along the trajectory. When computing the loss function (18), a subset of samples denoted by mini-batch \mathfrak{J} is randomly picked from \mathfrak{D} and used as the samples for gradient estimation. This method can improve the training efficiency by selectively reusing past samples. In addition, we advocate the *fixed target network* approach [24] by keeping the target network parameter fixed for several updates. To this end, let θ^- denote the target network parameter, which is only updated once every N_o iterations. This technique could mitigate any potential instability issue by changing the DQN target weights less frequently. By adopting *experience replay* method and *fixed target network* approaches, we obtain the estimates of loss function and its gradient as

$$\nabla_{\theta} \hat{\mathcal{L}}(\theta) = (1/|\mathfrak{J}|) \sum_{t \in \mathfrak{J}} \left[-2 \left(r_t + \gamma \max_{a_{t+1}} Q(s_{t+1}, a_{t+1}; \theta^-) - Q(s_t, a_t; \theta) \right) \nabla_{\theta} Q(s_t, a_t; \theta) \right]. \quad (20)$$

The detailed algorithmic steps for DQN-based OBC algorithm are tabulated in Algorithm 1. As mentioned earlier, the state variables p_t and f_t are not action dependent. Thus, their transitions are obtained from the profiles given as the algorithm input, such as real data provided by the market operators. For the convergence of DQN algorithms, the total number of iterations N is typically chosen to be large enough in practice. Note that Algorithm 1 can be used to search for the best policy under the linearized degradation cost as well, by using this simpler degradation cost model in (10). The ensuing section will compare these two degradation models numerically.

V. NUMERICAL TESTS

We have tested the proposed RL-based battery control algorithm for cycle-based degradation cost to the linearized approximation one [17]. Actual data of electricity market price and FR signal have been used, respectively from the ERCOT's market data depository [25] and PJM's ancillary service dataset [26]. Each time instance corresponds to a 5-minute interval. The FR signal is normalized to indicate either maximum charging or discharging for the battery. As mentioned in Remark 1, the fast FR signal at 1-minute rates is averaged over a 5-minute interval for the training phase, while the original data rate is maintained for the testing phase. We have used a 200kWh-capacity battery with (dis)charging

Algorithm 1: DQN-based Optimal Battery Control

1 Hyperparameters: discount factor $\gamma = 1$, learning rate $\eta > 0$, ϵ -greedy coefficient $\kappa \in (0, 1)$, mini-batch size $|\mathfrak{J}|$, target network update interval N_o , and maximum number of iterations N .

2 Input: training profiles of prices and FR signals with the exploration time horizon T .

3 Initialize: the ϵ -greedy probability $\epsilon \in (0, 1)$, replay memory $\mathcal{D} = \emptyset$, initial action-value function $Q(s, a; \theta')$ with a random θ' and the target network parameter $\theta^- = \theta'$ at iteration $n = 0$.

4 while $n \leq N$ **do**

5 for $t=0, \dots, T$ **do**

6 Select a random action a_t with probability ϵ ; otherwise, use the action $a_t^* = \arg \max_{a_t} Q(s_t, a_t; \theta')$.

7 Implement the action a_t to obtain the ensuing state s_{t+1} based on the transitions of both (4) and Table II, and by using the input profiles of p_{t+} and f_{t+1} .

8 Compute the instantaneous reward r_t in (14).

9 Store the tuple (s_t, a_t, s_{t+1}, r_t) in \mathcal{D} .

10 Select a random mini-batch \mathfrak{J} with size $|\mathfrak{J}|$ from \mathcal{D} .

11 Compute the gradient estimate using (20).

12 Update the parameter $\theta' \leftarrow \theta' - \eta \nabla \hat{L}(\theta')$.

13 **if** t/N_o *is an integer* **then**

14 Update the target network parameter $\theta^- \leftarrow \theta'$.

15 **end**

16 Update $\epsilon = \kappa \epsilon$.

17 **end**

18 Update the iteration number $n \leftarrow n + 1$.

19 end

limit of 10kW and minimum SoC of 20kWh. The parameters associated with battery degradation are set to $\alpha_d = 4.5 \times 10^{-3}$ and $\beta = 1.3$, as done in [19]. Examples profiles of normalized electricity market price and FR signal are depicted in Fig. 3.

The DQN **Algorithm 1** has been implemented in Python with the popular NN toolboxes Tensorflow and Keras [27]. Table III lists the parameter settings for the DQN training, which uses 7 daily profiles of $\{p_t, f_t\}$ at 5-minute rates. Hence, there are a total of 288 time instances for each exploration trajectory. Upon the convergence of Q-network, it is used to determine the optimal (dis)charging actions for each 1-minute interval of 60 days of testing data, while each testing trajectory having 1,444 time instances.

Training Comparisons. To compare the proposed cycle-based degradation cost with the linear one (denoted by CD and LD, respectively) in terms of battery control performance, We have considered three levels of degradation coefficients, at $0.5\alpha_d$, α_d , and $2\alpha_d$, respectively. Fig. 4 illustrates the training comparisons of the actual episode rewards (all based on cycle-based degradation) for all the three cases. Clearly, all the DQN iterations are convergent as the episode reward trajectories tend

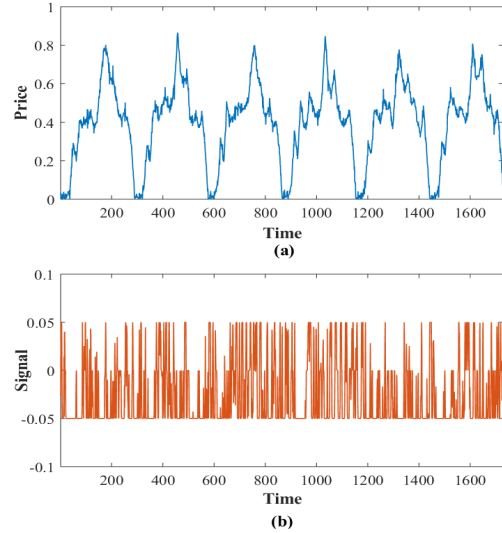


Fig. 3. Example profiles of normalized state variables: (a) electricity market price p_t and (b) FR signal f_t .

TABLE III
PARAMETER SETTINGS FOR DQN TRAINING

Parameter	Value
Number of hidden layers	2
Number of nodes	[128, 32]
Activation function	ReLU
Learning rate	0.001
Optimizer	Adam
Batch size (J)	64
Maximum number of iterations (N)	30000
Number of daily profiles	7

to be non-decreasing till reaching the highest values. Moreover, while the CD cases using our proposed *instantaneous cycle-based degradation* modeling outperform the LD counterparts, especially at larger degradation cost. This comparison validates the advantages of the proposed degradation model in terms of accurately representing the battery cost and thus leading to effective control policies.

Testing Comparisons. We have further compared the testing performance of the learned Q-networks using both CD and LD based models. Fig. 5 plots the total reward differences between the CD and LD solutions (positive differences indicating higher reward for CD) for each test trajectory under the three levels of degradation coefficients. The proposed CD based control leads to higher total reward for at least 61.67%, 73.33% or 78.33% of test scenarios, respectively for the three α_d levels. This result confirms the earlier observations in training phase that proposed solution is more attractive for larger degradation cost. Similar comparison is also observed in differences of battery degradation performance only (again, positive differences indicating lower degradation cost for CD), as illustrated by Fig. 6. Clearly, the proposed CD solutions overwhelmingly improve the battery degradation performance and accordingly the total reward, as compared to the existing LD-based approximation.

Fig. 7 plots the selected testing SoC trajectory to better illustrate the improvement of the proposed CD-based policy,

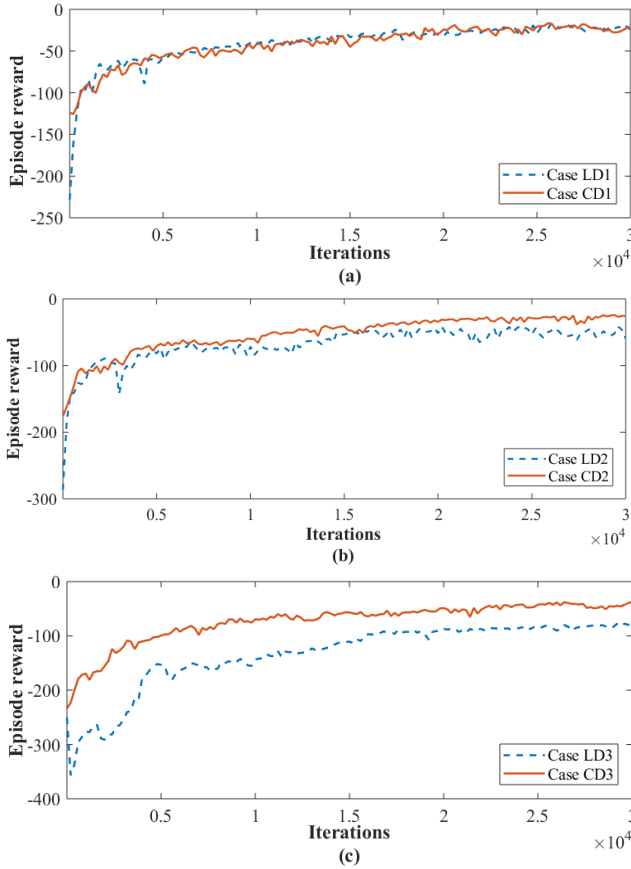


Fig. 4. Comparisons of the episode reward trajectory for (a) cases LD1 and CD1, (b) case LD2 and CD2, as well as (c) case LD3 and CD3.

corresponding to the two choices of degradation parameter ($0.5\alpha_d$ and α_d). Clearly, both trajectories show that the CD-based policy leads to better smoothness property of the long cycles as compared to the LD one, especially for the high-price period between [200, 800]. As explained in Sec. III, a single long and deep (dis)charging cycle is preferred for reducing the battery degradation, as opposed to having multiple shorter cycles, due to the exponential model for degradation cost in (8). The CD trajectory has one smooth and long discharging cycle during the high-price period, and this pattern is amendable to mitigating battery degradation. In contrast, the LD one has frequent, noticeable fluctuations during this period. Because of the linearized approximation, the LD-based policy leads to eight more noticeable (dis)charging cycles of considerate depth than the CD one. This speaks for the capability of the proposed CD model in effectively removing some unnecessary cycles of moderate depth, thanks to the accurate representation of rainflow-based degradation. In addition, in the post-peak period [1000, 1250], the LD based policy produces a couple of cycles of moderate depth which are not very profitable. The proposed CD based policy is able to successfully remove these non-profitable cycles and does not lead to any considerate cycles.

To sum up, the numerical results have validated the performance improvement attained by the proposed *instantaneous* cycle-based degradation cost model, in terms of capturing the

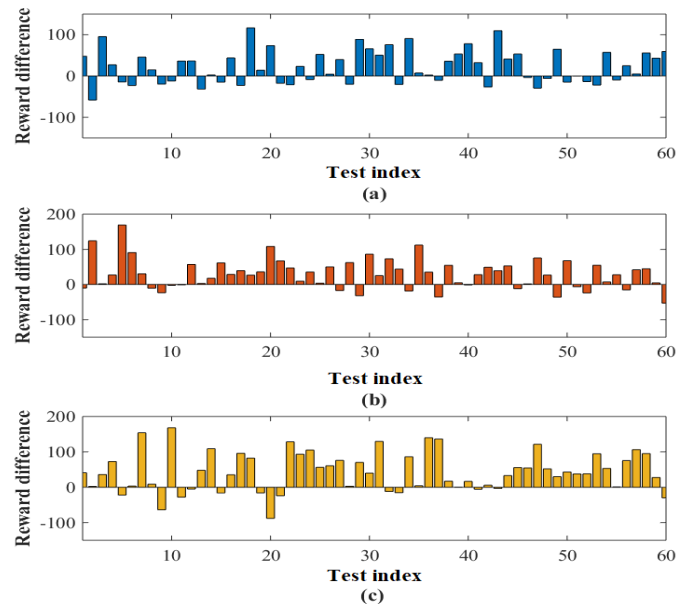


Fig. 5. The total reward differences (positive differences indicating higher reward for CD) between (a) cases LD1 and CD1, (b) cases LD2 and CD2, as well as (c) cases LD3 and CD3.

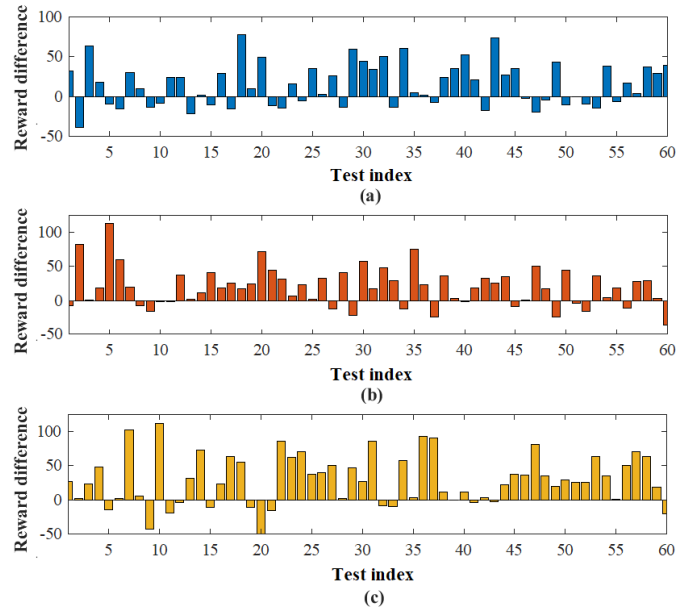


Fig. 6. The battery degradation differences (positive differences indicating lower degradation cost for CD) between (a) cases LD1 and CD1, (b) cases LD2 and CD2, as well as (c) cases LD3 and CD3.

characteristic of rainflow algorithm as the linearized approximation is unable to. As a result, the proposed solutions can effectively reduce the degradation-associated fluctuations and non-profitable (dis)charging cycles of the SoC trajectory.

VI. CONCLUSION AND FUTURE WORK

The paper proposes an accurate model of cycle-based degradation cost in order to allow for efficient battery control designs using reinforcement learning (RL). In order to model the degradation which depends on the full cycle, we introduce

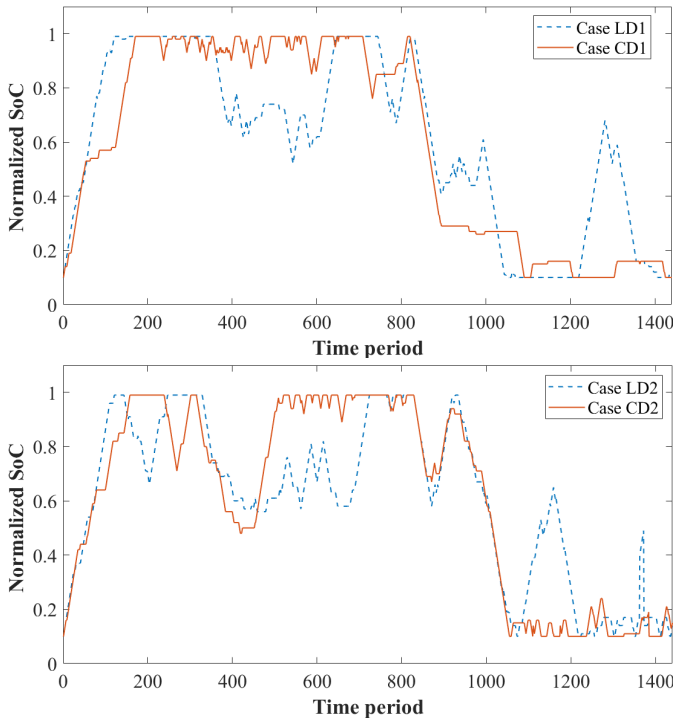


Fig. 7. Comparison of selected SoC trajectories between (a) cases LD1 and CD1, and (b) cases LD2 and CD2.

additional state variables to judiciously keep track of important switching points of SoC trajectory for effectively identifying (dis)charging cycles. This way, the actual degradation cost is separated into instantaneous terms along with other operation costs such as the net cost for electricity usage and FR penalty, such that powerful DQN based RL algorithms are readily applicable. Numerical tests confirm the effectiveness of proposed cycle-based degradation model and demonstrate the performance improvements in effectively mitigating battery degradation over existing linearized approximation approach.

Exciting future research directions open up on expanding the battery operations to support other ancillary services such as peak-shaving. The key question will be how to model the peak-shaving cost as instantaneous reward. In addition, the power network constraints such as voltage limit are of high interest in practice and will be considered as well.

REFERENCES

- [1] M. Arbabzadeh, R. Sioshansi, J. X. Johnson, and G. A. Keoleian, "The role of energy storage in deep decarbonization of electricity production," *Nature Communications*, vol. 10, no. 1, p. 3413, Jul 2019. [Online]. Available: <https://doi.org/10.1038/s41467-019-11161-5>
- [2] P. Denholm, E. Ela, B. Kirby, and M. Milligan, "Role of energy storage with renewable electricity generation," National Renewable Energy Lab (NREL), Tech. Rep., 2010.
- [3] D. Krishnamurthy, C. Uckun, Z. Zhou, P. R. Thimmapuram, and A. Botterud, "Energy storage arbitrage under day-ahead and real-time price uncertainty," *IEEE Transactions on Power Systems*, vol. 33, no. 1, pp. 84–93, 2018.
- [4] N. Padmanabhan, M. Ahmed, and K. Bhattacharya, "Battery energy storage systems in energy and reserve markets," *IEEE Transactions on Power Systems*, vol. 35, no. 1, pp. 215–226, 2020.

- [5] Y. Shi, B. Xu, Y. Tan, D. Kirschen, and B. Zhang, "Optimal battery control under cycle aging mechanisms in pay for performance settings," *IEEE Transactions on Automatic Control*, vol. 64, no. 6, pp. 2324–2339, 2019.
- [6] B. Xu, Y. Shi, D. S. Kirschen, and B. Zhang, "Optimal battery participation in frequency regulation markets," *IEEE Transactions on Power Systems*, vol. 33, no. 6, pp. 6715–6725, 2018.
- [7] Y. Shi, B. Xu, D. Wang, and B. Zhang, "Using battery storage for peak shaving and frequency regulation: Joint optimization for superlinear gains," *IEEE Transactions on Power Systems*, vol. 33, no. 3, pp. 2882–2894, 2018.
- [8] M. Vařak and G. Kujundžić, "A battery management system for efficient adherence to energy exchange commands under longevity constraints," *IEEE Transactions on Industry Applications*, vol. 54, no. 4, pp. 3019–3033, 2018.
- [9] S. Gupta, V. Kekatos, and W. Saad, "Optimal real-time coordination of energy storage units as a voltage-constrained game," *IEEE Transactions on Smart Grid*, vol. 10, no. 4, pp. 3883–3894, 2019.
- [10] T. Morstyn, B. Hredzak, R. P. Aguilera, and V. G. Agelidis, "Model predictive control for distributed microgrid battery energy storage systems," *IEEE Transactions on Control Systems Technology*, vol. 26, no. 3, pp. 1107–1114, 2017.
- [11] W. B. Powell and S. Meisel, "Tutorial on stochastic optimization in energy—part ii: An energy storage illustration," *IEEE Transactions on Power Systems*, vol. 31, no. 2, pp. 1468–1475, 2016.
- [12] B. Xu, A. Oudalov, A. Ulbig, G. Andersson, and D. S. Kirschen, "Modeling of lithium-ion battery degradation for cell life assessment," *IEEE Transactions on Smart Grid*, vol. 9, no. 2, pp. 1131–1140, 2018.
- [13] B. Recht, "A tour of reinforcement learning: The view from continuous control," *Annual Review of Control, Robotics, and Autonomous Systems*, vol. 2, no. 1, pp. 253–279, 2019. [Online]. Available: <https://doi.org/10.1146/annurev-control-053018-023825>
- [14] A. S. Zamzam, B. Yang, and N. D. Sidiropoulos, "Energy storage management via deep q-networks," in *2019 IEEE Power & Energy Society General Meeting (PESGM)*. IEEE, 2019, pp. 1–5.
- [15] J. Liu, H. Tang, M. Matsui, M. Takano, L. Zhou, and X. Gao, "Optimal management of energy storage system based on reinforcement learning," in *Proceedings of the 33rd Chinese Control Conference*, 2014, pp. 8216–8221.
- [16] B. V. Mbuwir, F. Ruelens, F. Spiessens, and G. Deconinck, "Battery energy management in a microgrid using batch reinforcement learning," *Energies*, vol. 10, no. 11, 2017. [Online]. Available: <https://www.mdpi.com/1996-1073/10/11/1846>
- [17] J. Cao, D. Harrold, Z. Fan, T. Morstyn, D. Healey, and K. Li, "Deep reinforcement learning-based energy storage arbitrage with accurate lithium-ion battery degradation model," *IEEE Transactions on Smart Grid*, vol. 11, no. 5, pp. 4513–4521, 2020.
- [18] R. Spotnitz, "Simulation of capacity fade in lithium-ion batteries," *Journal of Power Sources*, vol. 113, no. 1, pp. 72–80, 2003. [Online]. Available: <https://www.sciencedirect.com/science/article/pii/S0378775302004901>
- [19] Y. Shi, B. Xu, Y. Tan, and B. Zhang, "A convex cycle-based degradation model for battery energy storage planning and operation," in *2018 Annual American Control Conference (ACC)*, 2018, pp. 4590–4596.
- [20] R. S. Sutton and A. G. Barto, *Reinforcement Learning: An Introduction*, 2nd ed. The MIT Press, 2018. [Online]. Available: <http://incompleteideas.net/book/the-book-2nd.html>
- [21] T. Jónsson, "Forecasting and decision-making in electricity markets with focus on wind energy," Ph.D. dissertation, 2012.
- [22] D. Zhu and Y.-J. A. Zhang, "Optimal coordinated control of multiple battery energy storage systems for primary frequency regulation," *IEEE Transactions on Power Systems*, vol. 34, no. 1, pp. 555–565, 2019.
- [23] L.-J. Lin, "Self-improving reactive agents based on reinforcement learning, planning and teaching," *Machine Learning*, vol. 8, no. 3, pp. 293–321, May 1992. [Online]. Available: <https://doi.org/10.1007/BF00992699>
- [24] V. Mnih, K. Kavukcuoglu, D. Silver, A. A. Rusu, J. Veness, M. G. Bellemare, A. Graves, M. Riedmiller, A. K. Fidjeland, G. Ostrovski, S. Petersen, C. Beattie, A. Sadik, I. Antonoglou, H. King, D. Kumaran, D. Wierstra, S. Legg, and D. Hassabis, "Human-level control through deep reinforcement learning," *Nature*, vol. 518, no. 7540, pp. 529–533, Feb 2015. [Online]. Available: <https://doi.org/10.1038/nature14236>
- [25] Market Prices - ERCOT. <http://www.ercot.com/mktinfo/prices>. Accessed: 2021-06-29.
- [26] PJM Ancillary Services. <https://www.pjm.com/markets-and-operations/ancillary-services.aspx>. Accessed: 2021-06-29.
- [27] Keras. <https://github.com/fchollet/keras>. Accessed: 2021-06-29.